ACS EARTH AND SPACE CHEMISTRY

http://pubs.acs.org/journal/aesccq

Article

Negligible Role of Nitrate Radical in Directly Initiating Oxidation of Hg(0) to Hg(II) in the Atmosphere

Darshi T. Hewa Edirappulige, Lan Cheng, Hang Du, Zhengcheng Song,* Pedro J. Castro, Yanxu Zhang, and Theodore S. Dibble*

Cite This: *ACS Earth Space Chem.* 2026, 10, 868–879

Read Online

ACCESS | Metrics & More | Article Recommendations | Supporting Information

ABSTRACT: Nitrate radical (NO_3) has been suggested to participate in oxidizing gaseous Hg(0) in the atmosphere, most convincingly in the field study by Peleg et al. (*Environ. Sci. Technol.* 2015, 49, 14008–14018). This conclusion has been hard to reconcile with the two-step mechanism of Hg(0) conversion to Hg(II) via Hg(I), due to the low value reported for the NO_3–Hg(I) bond energy (~5 kcal mol^{-1}). Using a high level of computational quantum chemistry, we find this bond energy to be 6.5 kcal mol^{-1}, and we use standard statistical mechanics to compute the equilibrium constant, $K_c(T)$, for NO_3 + Hg(0) = NO_3Hg(I). Our kinetic analysis finds that under the conditions of Peleg et al., NO_3 could not have contributed significantly to the formation of Hg(II). In addition, we added NO_3-initiated oxidation of Hg(0) into the GEOS-Chem global model of atmospheric Hg. Despite that the model indicates that NO_3 oxidizes Hg(0) to Hg(I) about three times faster than either Br or OH radicals, NO_3Hg(I) falls apart so fast that NO_3-initiated oxidation has a negligible impact on atmospheric Hg cycling. Finally, we reanalyze an experiment that reported an upper limit to the rate constant for the NO_3 + Hg(0) reaction. We argue that this experiment would not have been able to detect the loss of Hg(0) due to gas-phase reaction with NO_3, even if this reaction proceeded with the collision rate constant.

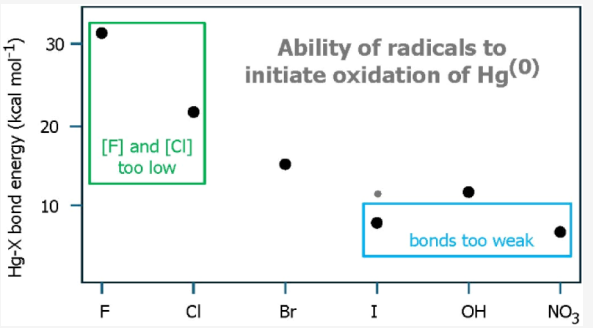

KEYWORDS: *gaseous elemental mercury, gaseous oxidized mercury, kinetics, quantum chemistry, global modeling*

INTRODUCTION

The atmosphere transports gaseous elemental mercury (Hg(0), GEM) globally, so that this neurotoxic pollutant is found in the poles as well as near its emission sources.[1] GEM deposits from the gaseous atmosphere roughly equally into vegetation versus oceans, in competition with reacting to form gaseous oxidized mercury (GOM), that is, Hg(II).[2,3] GOM, if not reduced back to GEM,[4,5] will deposit predominantly into oceans. The contrasting fates of GEM and GOM mean that we need to understand the redox chemistry of atmospheric mercury to predict when and where mercury enters ecosystems.

The major route for gas-phase oxidation of GEM to GOM in the troposphere and lower stratosphere is addition of a radical (Br, OH, or Cl) to form Hg(I) as a mercury-centered radical, which is further oxidized to Hg(II) by reaction with ozone, NO_2, or HOO.[6−18] Production of Br, OH, and Cl falls dramatically around sunset, so this mechanism does not explain multiple observations of elevated [GOM] at night. During nighttime, nitrate radical (NO_3) is the major oxidant for most volatile organic compounds,[19] so, naturally, atmospheric scientists have invoked NO_3 to explain elevated [GOM] at night.[20−23] Until recently, Peleg et al. had presented the most compelling evidence, namely, a strong correlation between measured nighttime [GOM] and [NO_3] in Jerusalem over the course of 6 weeks.[22] Unfortunately, there is very little kinetic or thermodynamic data to support these suggestions. Sommar et al.[24] reported an upper limit to the reaction:

$$\mathrm{Hg} + \mathrm{NO_3} \rightarrow \mathrm{Products} \quad (1)$$

at room temperature of $k_1 \leq 4 \times 10^{-15}$ cm^3 molecule^{-1} s^{-1} from flow-tube experiments at low pressure. Sumner et al.[25] briefly reported $k_1 \leq 7 \times 10^{-15}$ cm^3 molecule^{-1} s^{-1} from a chamber experiment at ambient pressure. Production of Hg(I)O + NO_2 in reaction (1) was later revealed to be highly endothermic (by ~45 kcal mol^{-1}),[26−29] as noted by Hynes et al.[30] As a result, it seems more likely that reaction (1) proceeds via formation of a weakly bound complex:

$$\mathrm{Hg} + \mathrm{NO_3} + M \rightleftarrows \mathrm{NO_3Hg(I)}\bullet + M \quad (2)$$

Received: December 7, 2025
Revised: January 20, 2026
Accepted: January 30, 2026
Published: February 17, 2026

(where M is a third body) mimicking the mechanism for other radicals:

$$\mathrm{Hg(0)} + Y + M \rightleftarrows Y\mathrm{Hg(I)}\bullet + M (Y = \mathrm{Br, OH, Cl}) \quad (3)$$

However, in 2012, quantum calculations by Dibble et al. reported D_0 (the bond energy at 0 K) for NO_3−Hg to be only 5.0 kcal mol^{-1}.[8] At the time, the only known pathway for oxidation of YHg(I)• to Hg(II) was via addition of radicals, •Z (Z = NO_2, HOO, halogen oxides, etc., but not NO):[8]

$$\mathrm{NO_3Hg(I)}\bullet + \bullet Z + M \rightarrow \mathrm{NO_3Hg(II)}Z + M \quad (4)$$

The weak bonding of NO_3Hg(I)• and the low concentrations of radicals, Z, in the atmosphere led Dibble et al. to conclude that NO_3 could not initiate oxidation of GEM to GOM.

The subsequent report, by Peleg et al., of a strong correlation between [NO_3] and [GOM][22] led us to consider two caveats to the conclusion of Dibble et al.[8] First, NO_3 radical is rather challenging for quantum chemistry,[31−36] and the calculations of Dibble et al. could easily be improved upon. Second, it had subsequently been realized that YHg(I)• could react with ozone with a rate constant approaching the collision limit:[11,37−39]

$$Y\mathrm{Hg(I)}\bullet + \mathrm{O_3} \rightarrow Y\mathrm{Hg(II)O}\bullet + \mathrm{O_2} \quad (5)$$

In work published before reaction (5) had been demonstrated to be important, it had been reported that OH initation would contribute <1% to GEM oxidation.[13] This small contribution was due to the weak HO−Hg bond (D_0 = 11.0 kcal mol^{-1}) of the HOHg(I)• intermediate, which caused it to dissociate to OH + Hg(0) before HOHg(I)• could react with radicals.[13] The abundance of ozone and the high rate constant for reaction (5) enables OH-initiation to contribute significantly (∼30%) to gross global production of GOM from GEM.[3,11] Typical nighttime [NO_3] is perhaps 20−100 times higher than typical daytime [OH],[40−43] and this higher concentration could help make NO_3 relevant to oxidation of GEM even if the NO_3−Hg(I) bond energy is somewhat lower than the HO−Hg(I) bond energy.

Below, we discuss the theoretical methods for our quantum calculations and the framework for modeling the global redox chemistry of atmospheric mercury. We then report the structure, vibrational spectrum, and bond energy of NO_3Hg(I)•, followed by the equilibrium constant of reaction (2) versus temperature. Next, we reanalyze the experiment of Sommar et al. to determine whether they could have detected loss of Hg(0). Following this, we investigate whether NO_3-initiated oxidation of GEM can explain the observations of Peleg et al. Finally, we use a global 3-D atmospheric transport and chemistry model (GEOS-Chem) to evaluate the contribution of this pathway to the global atmospheric cycling of Hg.

METHODS

Quantum Chemistry Calculations

Our quantum chemistry calculations aim for an accurate D_0 for NO_3Hg in order to reliably calculate the equilibrium constant for reaction (2). The electronic structure of NO_3 poses major challenges for quantum chemistry calculations because of its multireference character and symmetry breaking due to pseudo-Jahn−Teller coupling in its open-shell electronic states.[33−36] On the other hand, the NO_3 anion has a simple closed-shell electronic ground state. Equation-of-motion ionization potential coupled-cluster (EOMIP-CC)[44,45] calculations using the closed-shell ground state of NO_3^- as the reference state and removing an electron to obtain NO_3 has been shown to provide an accurate description for low-lying electronic states of NO_3.[46,47] We follow this prescription here and perform calculations of NO_3 and $HgNO_3$ using the EOMIP-CC singles and double (CCSD)[44,45] and CC singles doubles triples (CCSDT) methods.[48,49] The spin-free exact two-component theory in its one-electron variant (the SFX2C-1e scheme)[50−52] has been used to treat scalar-relativistic effect. The equilibrium structures and harmonic vibrational frequencies of NO_3 and NO_3Hg have been calculated with the valence electrons correlated using triple-ζ quality atomic natural orbital (ANO-RCC1) basis sets using the primitive functions of the ANO-RCC sets[53−55] recontracted for the SFX2C-1e calculations using CCSD density matrices. We have performed calculations of harmonic vibrational frequencies to confirm that the optimized structure corresponds to a stable structure on the potential energy surface.

To refine the NO_3−Hg bond energies, we carried out EOMIP-CCSD calculations with more complete treatments of basis-set and electron-correlation effects. These calculations have correlated valence and semicore electrons, including the Hg 4f5s5p5d6s, N 2s2p, and O 2s2p electrons. We used uncontracted triple-ζ (TZ) and quadruple-ζ (QZ) basis sets for Hg constructed using primitive functions of the ANO-RCC sets and correlation-consistent sets[56] as well as aug-cc-pVTZ and aug-cc-pVQZ sets for N and O[57] recontracted for the SFX2C-1e scheme. The basis-set-limit (∞Z) EOMIP-CCSD energies were obtained by combining the QZ Hartree−Fock energies with basis-set-limit values for the EOMIP-CCSD electron-correlation and ionization energies estimated by extrapolating the TZ and QZ results using a simple two-point formula.[58] The contributions due to the correlation of deep inner-shell electrons were estimated by performing EOMIP-CCSD/TZ calculations with the correlation of Hg 4s, 4p, 4d and O 1s orbitals. Furthermore, the contributions from triple excitations were obtained as the differences between EOMIP-CCSDT and CCSD results using the ANO-RCC1 basis sets. We also carried out EOMIP-CCSD calculations with spin−orbit coupling to obtain the second-order spin−orbit (SO) contributions to D_0. Here, the X2C Hamiltonian[50,51,59] with atomic mean field[60] integrals (the X2CAMF scheme)[61,62] has been used to provide variational treatments of spin−orbit coupling. We have used the recent implementation of the X2CAMF EOM excitation energy (EOMEE)-CCSD method[63] together with the continuum orbital trick[48] for these X2CAMF-EOMIP calculations. The SO contribution to D_0 obtained from these calculations is less than 0.1 kcal/mol and thus insignificant for the present discussion. The basis sets used in the calculations described here are documented in the Supporting Information. All calculations were performed using the CFOUR program package.[64]

We calculated the equilibrium constant for reaction (2) vs temperature (200−320 K) from D_0 with the *thermo* program in the MultiWell program suite,[65−67] using the rigid rotor-harmonic oscillator approximation.

Our goal for understanding the oxidation of NO_3Hg(I)• by radicals (NO_2, HOO, BrO, NO_3, and O_2) and ozone is to verify that these reactions occur similarly to those of HOHg(I)• and BrHg(I)•. While this requires reliable levels of theory, it does not require the precision needed in determining D_0 for NO_3Hg. All thermochemical calculations with DFT methods were performed using Gaussian 16[68] to ensure consistency in the computed energetics. Bond scans for assessing the presence or absence of energy barriers were conducted using ORCA 5.0.3.[69,70] Density functional theory (DFT) was used to optimize geometries and compute harmonic vibrational frequencies. We used three functionals that have proven reliable in our previous studies of mercury chemistry: CAM-B3LYP[71] (with D3BJ dispersion correction),[72] PBE0,[73] and M06−2X.[74] For H, N, and O atoms, we used Dunning's aug-cc-pVTZ basis set.[75,76] To account for scalar relativistic effects in Hg and Br, we used the Stuttgart/Cologne small-core pseudopotentials (ECPMDF60 and ECPMDF10, respectively), while the electrons outside the pseudopotential were described with

https://doi.org/10.1021/acsearthspacechem.5c00382
ACS Earth Space Chem. 2026, 10, 868−879

Table 1. Chemical Mechanism and Rate Constants for NO3-Initiated Oxidation of Mercury and Reactions of the Subsequent Products

Reaction	Rate Coefficients	References
$Hg(0) + NO_3 + M \rightarrow NO_3Hg(I) + M$	$k_0 = 1.0 \times 10^{-32}\ (298/T)^2$	This study[a]
$Hg(I)NO_3 + M \rightarrow Hg(0) + NO_3 + M$	k_0/K_c; $K_c = 1.0 \times 10^{-24}\ \exp(3305/T)$	This study
$Hg(I)NO_3 + O_3 \rightarrow NO_3Hg(II)O + M$	$k_2(T) = 7.5 \times 10^{-11}$	This study
$Hg(I)NO_3 + NO_2 \rightarrow NO_3Hg(II)ONO + M$	$k_3((M), T) = 4.3 \times 10^{-30}\ (T/298)^{-5.9}$	By analogy to BrHg(I) + NO_2[b]
$Hg(I)NO_3 + Z + M \rightarrow NO_3Hg(II)Z + M$ Z = (HOO, XO, X, where X = Cl, Br)	$k_4((M), T) = 1/2 \times K_3((M), T)$	This study
$NO_3Hg(II)O + CH_4 \rightarrow NO_3Hg(II)OH$	$4.1 \times 10^{-12}\ \exp(-856/T)$	By analogy to BrHg(II)O + CH_4[b]
$NO_3Hg(II)O + CO \rightarrow Hg(I)NO_3 + CO_2$	$6.0 \times 10^{-11}\ \exp(-550/T)$	By analogy to BrHg(II)O + CO[b]
$NO_3Hg(II)ONO + h\nu \rightarrow NO_3Hg(II)O + NO$	$\Phi = 0.90$, $J\ (s^{-1}) = 1.1 \times 10^{-3}$	J and products by analogy to BrHg(II)ONO[b]
$NO_3Hg(II)HO_2 + h\nu \rightarrow NO_3Hg(II)O + Hg(0) + Hg(I)NO_3 + NO_3Hg(II)OH + NO_3$	$\Phi = 0.66$, $J\ (s^{-1}) = 1.5 \times 10^{-2}$	J and products by analogy to BrHg(II)HO_2[b]
$NO_3Hg(II)OBr + h\nu \rightarrow NO_3Hg(I) + BrO$	$\Phi = 1.00$, $J\ (s^{-1}) = 2.4 \times 10^{-2}$	J and products by analogy to BrHg(II)BrO[b]
$NO_3Hg(II)OCl + h\nu \rightarrow NO_3Hg(I) + ClO$	$\Phi = 1.00$, $J\ (s^{-1}) = 1.4 \times 10^{-2}$	J and products by analogy to BrHg(II)BrO[b]
$NO_3Hg(II)Br + h\nu \rightarrow Hg(0) + Br + Hg(I)NO_3$	$\Phi = 0.40$, $J\ (s^{-1}) = 1.2 \times 10^{-6}$	J and products by analogy to Hg(II)Br_2[b]
$NO_3Hg(II)OH + h\nu \rightarrow Hg(0) + NO_3 + OH$	$\Phi = 0.49$, $J\ (s^{-1}) = 1.3 \times 10^{-5}$	J and products by analogy to BrHg(II)OH[b]

[a]Assuming k(1 atm, 298 K) = 10^{-16} cm^3 molec^{-1} s^{-1} and the reaction is in the low-pressure limit. [b]The redox and photolysis rates are set to the values for the analogous Br-compounds reported in Shah et al. (2021).

the aug-cc-pVTZ-PP basis set of Peterson and coworkers.[56,77,78] Our shorthand for this combination of basis sets is AVTZ. All radicals were treated with spin-unrestricted wave functions, and we verified the stability of the wave functions. Spin−orbit corrections to relative energies should be modest (<1 kcal mol^{-1}) except for reactions involving BrO.[79,80]

Atmospheric Modeling

We employed the GEOS-Chem model (version 12.9.0),[81] incorporating Hg chemistry developed by Shah et al.,[3] in which Br and OH radicals are the primary oxidants for the conversion of atmospheric Hg(0) to Hg(II). Atmospheric Hg(II) may partition into aerosols and cloud droplets, and both gaseous and heterogeneous Hg(II) can be reduced back to Hg(0). The model operates at a spatial resolution of 4° latitude by 5° longitude, with 47 vertical layers, and is driven by the MERRA2 reanalysis of meteorological data. Anthropogenic emissions are sourced from Streets et al.[82] and further refined by Zhang et al.,[83] while natural emissions are based on Horowitz et al.[14] The model also includes dynamic coupling between the atmosphere and Earth's surface, using gridded land and ocean Hg concentrations as boundary conditions. Atmospheric Hg is deposited to Earth's surface via both dry and wet deposition. For Hg(0) over land, dry deposition velocity is calculated using a resistance-in-series scheme.[84] The exchange of Hg(0) between the atmosphere and ocean is governed by the air-sea exchange model.[85] Both gaseous and particle-bound Hg(II) undergo deposition through dry and wet processes, as described by integrated schemes.[85−88]

We integrated NO_3-initiated redox reactions into the model's kinetic preprocessor. These reactions are analogous to those initiated by Br and OH, with O_3 acting as the primary oxidant converting of Hg(I) to Hg(II) (in the form of YHg(II)O•). YHg(II)O• can react with CH_4 and other volatile organic compounds (VOCs) to form thermally stable YHg(II)OH or be reduced (mostly by CO) back to YHg(I)•. The NO_3 concentrations were retrieved from archived full-chemistry simulations in the GEOS-Chem model (version 14.5.1).[89] Rate constants for the NO_3-initiated redox reactions are summarized in Table 1. The model simulation spans from 2013 to 2017, with the first four years used for model initialization and the fifth year for result analysis.

RESULTS AND DISCUSSION

Hg Binding to NO_3 Radical

We initially optimized a C_{2v} structure of $NO_3Hg(I)$•, but this turned out to be a transition state (denoted TS-$NO_3Hg(I)$•) at both the DFT/AVTZ (for all three functionals) and SFX2C-1e-EOMIP-CCSD(T)/ANO-RCC1 levels of theory. Instead, $NO_3Hg(I)$• adopts a structure of C_s symmetry with the Hg atom binding asymmetrically (2.20 vs 2.56 Å) to two of the O atoms of NO_3 (see Figure 1). Vibrational frequencies are listed in Tables S3 and S4 of the Supporting Information.

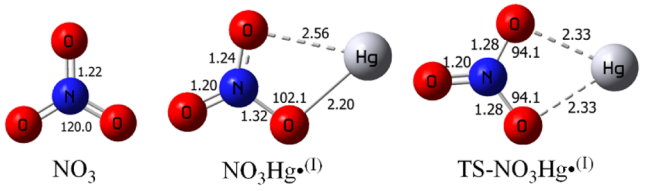

Figure 1. Structures of NO_3 (D_{3h}), $NO_3Hg(I)$• (C_s), and TS-$NO_3Hg(I)$• (C_{2v}) at SFX2C-1e-EOMIP-CCSD/ANO-RCC1 level. Angles and bond distances are listed in degrees and Å, respectively.

We computed the NO_3−Hg bond energy at 0 K (D_0) as 6.5 kcal mol^{-1}, which is 1.5 kcal mol^{-1} higher than the value computed previously by Dibble et al.[8] There are multiple contributors to this difference, including that Dibble et al. used lower levels of theory for structures and energies, and smaller basis sets for evaluating the energy.[8]

Let us consider the uncertainty in our value of D_0. As shown in Table S2, the difference between the D_0 values obtained from ∞Z and QZ calculations is about 1 kcal mol^{-1}. The remaining basis-set effects are likely substantially smaller. The contribution to D_0 from the correlation of the inner-shell electrons is around 0.5 kcal mol^{-1}. The remaining errors due to the correlation of even deeper electrons are expected to be insignificant. The triples contribution to D_0 amounts to around 0.5 kcal mol^{-1}. The remaining electron-correlation contribu-

https://doi.org/10.1021/acsearthspacechem.5c00382
ACS Earth Space Chem. 2026, 10, 868−879

tion due to quadruple excitations is expected to be smaller than the triples contributions. Based on the trends in these results, we estimate the uncertainty in the contribution from electronic energies to the value of D_0 as around 1 kcal mol^{-1}.[26,27,41,42,78] Values of K_c are computed from standard statistical mechanics

Table 2. Temperature Dependence of the Equilibrium Constant (K_c, cm^3 molecule^{-1}) Based on SFX2C-1e-EOMIP-CCSDT/ANO-RCC1 for Energies, CCSD/ANO-RCC1 for Rotational Constants, and Experimental Values of Vibrational Frequencies

T (K)	K_c
200	1.5×10^{-17}
220	3.3×10^{-18}
240	9.6×10^{-19}
260	3.3×10^{-19}
280	1.3×10^{-19}
298.15	6.5×10^{-20}
300	6.1×10^{-20}
320	3.1×10^{-20}

for the range 200 K ≤ T ≤ 320 K and displayed in Table 2. We fit the values to an Arrhenius expression:

$$K_c(T) = 1.0 \times 10^{-24} e^{+3305/T} \text{cm}^3\text{molecule}^{-1} \quad (6)$$

with less than 1% deviation from the values in Table 2. Because vibrational frequencies of NO_3 are challenging to compute accurately, we calculated $K_c(T)$ using the observed vibrational frequencies as tabulated in the MultiWell Thermodynamics Database[90] rather than the values we computed at SFX2C-1eEOMIP-CCSD/ANO-RCC. Using the calculated vibrational frequencies lowered K_c modestly, by 9% to 16% for 200 K ≤ T ≤ 320 K. Using the vibrational energy levels of Eisfeld (see Text S2 in the Supporting Information) raised K_c by 2.4% at 200 K and lowered K_c by 4.2% at 320 K, with a monotonic progression between those two temperatures. These uncertainties in K_c are much smaller than those due to the uncertainty in D_0 (1 kcal mol^{-1}, causing a factor of 5 uncertainty at 298 K). As we show below, this uncertainty will not change the conclusions of our analysis of the laboratory kinetics experment[23] or the field study of Peleg et al.[22]

Bimolecular Reactions of $NO_3Hg(I)$•

We investigated the reactions of $NO_3Hg(I)$• with ozone and with some of the more abundant radicals in the atmosphere: Z = O_2, NO_2, HOO, NO_3, and BrO. To help analyze the experimental work of Sommar et al.[24] we also studied the reactions of NO_3Hg with NO_3 and HNO_3 (see Text S3 in the Supporting Information).

As can be seen from Table 3, bond energies (D_0) of $NO_3Hg(I)$• to several atmospherically abundant radicals, •Z, are slightly lower than those for HOHg-Z and BrHg-Z; we previously showed the near-equivalence of HOHg-Z and BrHg-Z bond energies.[13] For NO_3Hg-NO_3, for which no $HOHgNO_3$ or $BrHgNO_3$ analogs are in the literature, the bond energy is 64.4 kcal mol^{-1}. In Figure 2 we show the correlation of the bond energies of NO_3Hg-Z and HOHg-Z. We verified that these radical−radical addition reactions proceed without a barrier, except in the case of Z = O_2. Note that previous calculations established the presence of a barrier to $BrHg + O_2 + M \rightarrow BrHgOO + M$.[5]

Table 3. YHg-Z Bond Energies D_0, kcal mol^{-1} Calculated at the PBE0/AVTZ Level of Theory (Y = NO_3, OH, Br and Z = NO_2, HOO, BrO, O_2)

Reaction	NO_3Hg	HOHg	BrHg
$YHg + NO_2 \rightarrow$ *syn*-$YHgONO$	−35.2	−38.9	−36.4
$YHg + NO_2 \rightarrow$ *anti*-$YHgONO$	−28.1	−33.0	−29.1
$YHg + NO_2 \rightarrow YHgNO_2$	−30.8	−35.3	−31.4
$YHg + OOH \rightarrow YHgOOH$	−35.3	−38.6	−35.1
$YHg + OBr \rightarrow YHgOBr$	−47.5	−51.9	−50.8
$YHg + O_2 \rightarrow YHgO_2$	−4.5	−8.6	−5.4

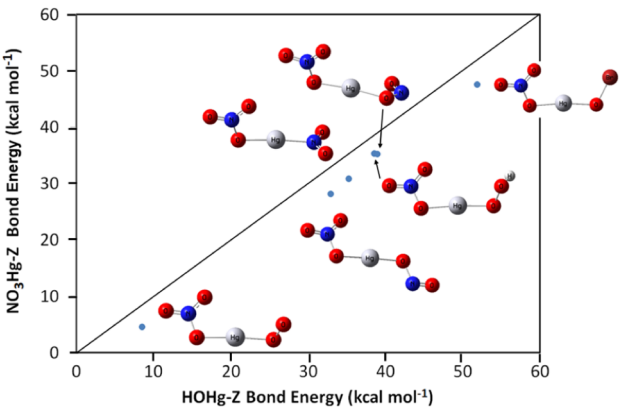

Figure 2. Plot of bond energies (D_0) for NO_3Hg-Y versus HOHg-Y for Y = O_2, NO_2, HOO, and BrO at PBE0/AVTZ, along with structures of the NO_3HgZ compounds. The Figure includes the 1:1 line to highlight the deviation between HOHg-Z and NO_3Hg-Z bond energies.

Reaction of NO_3Hg with ozone to produce $NO_3Hg(II)O$• + O_2 is significantly exothermic (ΔH_r°(0 K) = −46.3 kcal mol^{-1} and possesses no barrier. This suggests that the rate constant for this reaction may, like those for BrHg(I)• + O_3 and HOHg(I)• + O_3, approaches the collision limit at room temperature.[11,37−39] This suggests that the major bimolecular reaction of $NO_3Hg(I)$• (like HOHg(I)• and BrHg(I)•) is reaction with ozone.[3]

Reanalyzing the Experimental Study of k(Hg + NO_3)

Sommar et al. used a fast-flow discharge reactor to investigate the rate constant for Hg(0) + NO_3 at total pressures of 5.4−9.4 mbar of He. Based on previous work using the same reactor at similar pressures, the flow velocity in the reactor probably exceeded 100 cm sec^{-1}.[91] Given the total reactor length of 1 m, this leads to reaction time of less than one second. Nitrate radical was produced from F + HNO_3 before Hg entered the reactor, and was present (8−17 × 10^{12} molecules cm^{-3}) in excess over Hg(0) (0.7−2.1 × 10^{12} molecules cm^{-3}). Sommar et al. assumed that reaction of NO_3 with Hg(0) was irreversible on the time scale of the experiment. This assumption was not unreasonable given the erroneous data then available on ΔH_f^0 for gaseous HgO, from which it was concluded that the following reaction was thermodynamically favorable:

$$Hg + NO_3 \rightarrow HgO + NO_2 \quad (7)$$

However, four quantum chemical studies using three different approaches show that HgO is very weakly bound (3−6 kcal mol^{-1}),[26−29] which renders (7) so endothermic ($\Delta H_r^\circ \approx$ +45 kcal mol^{-1}) that it will not occur. Instead, the reaction must proceed to form $NO_3Hg(I)$•. If $NO_3Hg(I)$•

https://doi.org/10.1021/acsearthspacechem.5c00382
ACS Earth Space Chem. 2026, 10, 868−879

rapidly falls apart to regenerate Hg(0), the upper limit reported by Sommar et al. might not be valid. Therefore, we next consider whether reactions of $NO_3Hg(I)\bullet$ with NO_3 or HNO_3 could compete with dissociation of $NO_3Hg(I)\bullet$ to NO_3 + Hg(0).

$NO_3Hg(I)\bullet$ could react with HNO_3 via:

$$NO_3Hg(I)\bullet + HNO_3 \rightarrow NO_3Hg(II)H + NO_3 \quad (8a)$$

$$NO_3Hg(I)\bullet + HNO_3 \rightarrow Hg(II)(NO_3)_2 + H \quad (8b)$$

We find these reactions to be significantly endothermic (at CAM-B3LYP-D3BJ/AVTZ). ΔH_r^0(0 K) is +24 kcal mol^{-1} for (8a) and +39 kcal mol^{-1} for (8b). We calculate an upper limit to the rate constant for the less endothermic reaction channel (8a). The estimate is made via $k_{8a}(T) = Ae^{-E_a/RT}$, taking ΔH_r^0(0 K) as a lower limit to E_a and 10^{-10} cm^3 molecule^{-1} s^{-1} as the upper limit to A. This approximation gives $k_{8a}(298) < 10^{-27}$ cm^3 molecule^{-1} s^{-1}. If we assume that the DFT value of ΔH_r^0(0 K) exceeds the true value by as much as 10 kcal mol^{-1}, we get $k_{8a}(298) < 10^{-21}$ cm^3 molecule^{-1} s^{-1}. The HNO_3 concentration was not given, but must have been a modest fraction of the total pressure of 9.4 mbar (2.3×10^{17} molecules cm^{-3}). Using the upper limit to k_{8a}, and $[HNO_3]$ = 9.4 mbar, the pseudofirst order rate constant ($k_{8a}' = k_{8a}[HNO_3]$) for $HgNO_3$ loss lies below 10^{-3} s^{-1}, corresponding to a lifetime greater than 1000 s. Clearly, HNO_3 did not contribute to gas-phase loss of $HgNO_3$ in the available reaction time of 1 s.

As discussed above, $NO_3Hg(I)\bullet$ can react with NO_3 without a barrier to make $Hg(II)(NO_3)_2$:

$$NO_3Hg(I)\bullet + NO_3 + M \rightarrow Hg(II)(NO_3)_2 + M \quad (9)$$

We created a kinetic model of the fate of GEM in the experiment using the computer program Kintecus.[92,93] We simulated the gas-phase formation and dissociation of $NO_3Hg(I)\bullet$ (reactions 2 and −2) along with reaction (9) over 1 s, equal to our estimate of the longest reaction time in the experiment. We set k_9 at 10^{-10} cm^3 molecule^{-1} s^{-1} to maximize the opportunity for formation of Hg(II); given the low pressure in the experiment, this value of k_9 almost certainly exceeds the effective second-order rate constant for this termolecular reaction. We varied k_2 between 10^{-10} and 10^{-18} cm^3 molecule^{-1} s^{-1} and computed k_{-2} from the 298 K equilibrium constant for reaction 2 (see Table 1). For $k_2 > 5 \times 10^{-15}$ cm^3 molecule^{-1} s^{-1}, the concentration of $NO_3Hg(I)\bullet$ was controlled by equilibrium to within 1%, and the loss of GEM was less than 0.2% at 1 s. Figure 3 depicts the time evolution [Hg(0)], $[NO_3Hg(I)\bullet]$, and $[Hg(II)(NO_3)_2]$ under these conditions. Such small fractional losses of GEM would not have been observable by Sommar et al. against the wall loss that dominated their experiment. Even if K_c was ten times higher than computed here, the simulated gas-phase loss of GEM would have been only 1.4%, resulting in gas-phase loss of GEM that would be less than 3% of the loss of GEM to the walls at their lower S/V for the one-second reaction time. Given the reported 20% uncertainty in the effective second-order rate constant for wall loss under these conditions, this small extent of gas-phase loss would not have been noticeable. Therefore, the work of Sommar et al. does not constrain the value of k_2.

Figure 4 shows how the assumed value of k_2 affects predicted values of steady state $[NO_3Hg(I)\bullet]$, the fraction of $NO_3Hg(I)\bullet$ reacting with NO_3, and the rate of loss of GEM in the experiment of Sommar et al. While decreasing k_2 below 10^{-15} cm^3 molecule^{-1} s^{-1} increases the fraction of $NO_3Hg(I)\bullet$

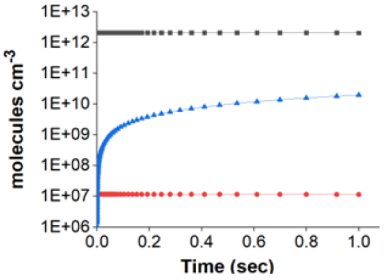

Figure 3. Simulated time evolution of [Hg] (■), $[NO_3Hg(I)\bullet]$ (● (red)), and $[Hg(II)(NO_3)_2]$ (▲ (blue)) in the experiment of Sommar et al.[24] This simulation used $[Hg(0)]_0 = 2.1 \times 10^{12}$ molecules cm^{-3} and $[NO_3]_0 = 1.7 \times 10^{13}$ molecules cm^{-3}, which were the highest concentrations used in the experiment.

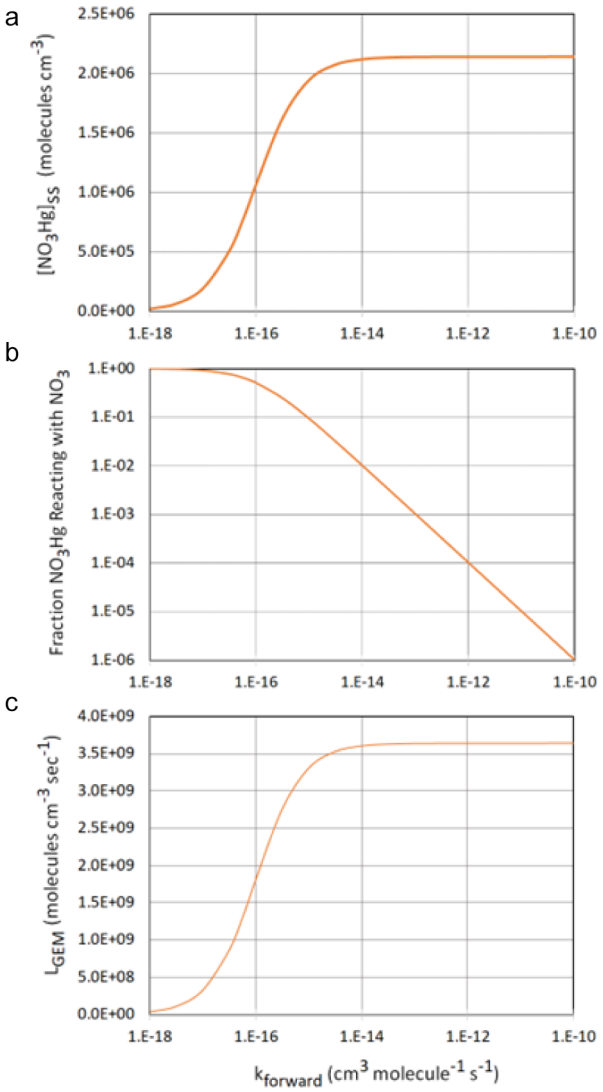

Figure 4. Simulation results for the experiments of Sommar et al.[24] Variation in a) steady state $[NO_3Hg]$, b) fraction of NO_3Hg making $Hg(NO_3)_2$, and c) rate of production of $Hg(NO_3)_2$ (equals the rate of loss of GEM, L_{GEM}), versus the assumed value of k_2 (= $k_{forward}$ (P,T) for $NO_3 + Hg \rightarrow NO_3Hg$). The effective second-order rate constant, k_9, for $NO_3Hg + NO_3Hg \rightarrow Hg(NO_3)_2$ was set to 10^{-10} cm^3 molecule^{-1} s^{-1}.

https://doi.org/10.1021/acsearthspacechem.5c00382
ACS Earth Space Chem. 2026, 10, 868−879

reacting with NO_3, this decreases steady state [$NO_3Hg(I)\bullet$] and, therefore, reduces the rate of loss of GEM.

Note that Sumner et al. briefly reported upper limits to k_2 of $7-30 \times 10^{-15}$ cm^3 molecule^{-1} s^{-1} in chamber experiments.[25] They did not report any concentration data that would allow us to simulate the conditions of their experiment. Given that k_2 is expected to be pressure-dependent, its value under the conditions of Sumner et al. (in 1 atm of air) would probably greatly exceed its value under the conditions of Sommar et al. (in 0.05−0.1 atm of He).

NO_3-Initiated Oxidation of GEM Cannot Explain Nighttime GOM Production in Peleg et al.

Peleg et al. reported strong correlations between nighttime [GOM] and [NO_3] over their six-week study period, but an absence of correlation with [GEM], [particulate mercury], [O_3], [CO], [SO_2], [sulfate], or wind direction.[22] Citing the argument of Dibble et al.[8] that the instability of $NO_3Hg(I)\bullet$ would prevent it from initiating oxidation of GEM, Peleg et al. were careful to suggest that NO_3 was "involved" in GEM oxidation, rather than initiating GEM oxidation. However, there are only two known roles for oxidants in Hg(II) production: either initiation to form Hg(I) or oxidation of Hg(I) to Hg(II). Subsequent to the publication of Peleg et al., it was learned that ozone can oxidize Hg(I) to Hg(II) with a high rate constant.[11,37−39] Clearly, the 69 ± 75 ng m^{-3} of NO_3 present under the conditions of Peleg et al. could not measurably increase the rate of oxidation of Hg(I) over that caused by 90 ± 28 μg m^{-3} of ozone. So the only significant role for NO_3 in GEM oxidation would be initiation. Accordingly, to investigate the role of NO_3 in the oxidation of GEM to GOM, we simulated the potential for nitrate radical to initiate production of GOM with the following mechanism:

$$Hg + NO_3 + M \rightleftarrows NO_3Hg(I)\bullet + M(k_2, k_{-2})$$

$$NO_3Hg(I)\bullet + O_3 \rightarrow NO_3Hg(II)O\bullet + O_2(k_7)$$

This mechanism allows us to calculate P_{GOM}, the gross rate of production of GOM. Our mechanism omits the subsequent reactions of $NO_3Hg(II)O\bullet$. By analogy to $HOHg(II)O\bullet$ and $BrHg(II)O\bullet$, we presume that reactions of $NO_3Hg(II)O\bullet$ with volatile organic compounds (VOCs) and NO_x would lead to the formation of closed-shell GOM compounds.[94−96] But reaction of $NO_3Hg(II)O\bullet$ with CO would yield $NO_3Hg(I)\bullet$,[96,97] thereby reducing [GOM] below the total [$NO_3Hg(II)O\bullet$] produced. We cannot address these competing processes due to the absence of data on either the concentrations of CO and VOCs at Peleg's study site or the rate constants for these reactions.[62,63] Of course, deposition and heterogeneous uptake on aerosol would also cause loss of GOM at an unknown rate. As a result, what we calculate is the integrated production of GOM over the course of 12 h (P_{GOM} × 43,200 s). This concentration exceeds the actual [GOM] that would exist at any point during the night as a result of NO_3-initiated oxidation of GEM.

We selected simulation conditions and rate constants that bias our simulations toward high production of GOM. Specifically, we used the highest values of reactant concentrations reported by Peleg et al.: [Hg(0)] = 2.6 ng m^{-3} (7.8×10^6 molecules cm^{-3}), [NO_3] = 430 ng m^{-3} (4.2×10^9 molecules cm^{-3}), and [O_3] = 200 μg m^{-3} (2.5×10^{12} molecules cm^{-3}). Despite these choices biasing the simulation to *over*estimate GOM production, GOM production was only 1.7×10^4 molecules cm^{-3} (5.6 pg m^{-3}), which is much less than the average observed [GOM] of 24 pg m^{-3}, let alone the peak values of >90 pg m^{-3}. Furthermore, the simulations held [GEM], [NO_3], and [O_3] constant, while their reported concentrations varied considerably during a single night.[22] Note that the rate of GOM production in this case is proportional to [GEM] × [NO_3] × [O_3]; by using the maximum concentrations, we overestimate GOM production by a factor of 20. So, the factor of 5 uncertainty in K_c cannot have caused us to underestimate the average extent of GOM production initiated by NO_3. In addition, we used $k_2 = k_5 = 10^{-10}$ cm^3 molecule^{-1} s^{-1}, that is, near the collision limit. This value may not be unreasonable for k_5 (with Y=NO_3),[11,37−39] but this value of k_2 exceeds the rate constants for the analogous reactions forming $BrHg(I)$[98] and $HOHg(I)$[99,100] by factors of ∼300 and ∼1000, respectively (at 1 atm near 298 K). Finally, the KCl denuder used to trap GOM in the field study is now known to underestimate the true concentration of GOM by a factor of 2 to four.[101−104] So the true values of [GOM] under the conditions of the study by Peleg et al. were likely much higher than the measured values. As a result, we conclude that gas-phase reaction of NO_3 with GEM contributed, at most, very little to formation of the GOM observed by Peleg et al. Figure S5 in the Supporting Information illustrates how the assumed value of k_2 affects steady state [$NO_3Hg(I)\bullet$], the fraction of $NO_3Hg(I)\bullet$ reacting with NO_3, and the rate of production of GOM in the field study.

Our analysis of Peleg et al. only considered gas-phase chemistry. One might invoke surface reactions to explain their observations, especially considering that surface reactions dominated the loss of GEM in the experiment of Sommar et al. However, the Hg(II) produced on surfaces would have to be emitted to the gas phase to be detected by Peleg et al.

Contribution of Hg(0) + NO_3 to Global Atmospheric Hg Oxidation

Figure 5 presents the global redox rates from the model incorporating the NO_3 pathway (NO_3-initiated oxidation reaction of GEM and the subsequent redox reactions). Although oxidation of Hg(0) to Hg(I) by NO_3 (∼30 Gg

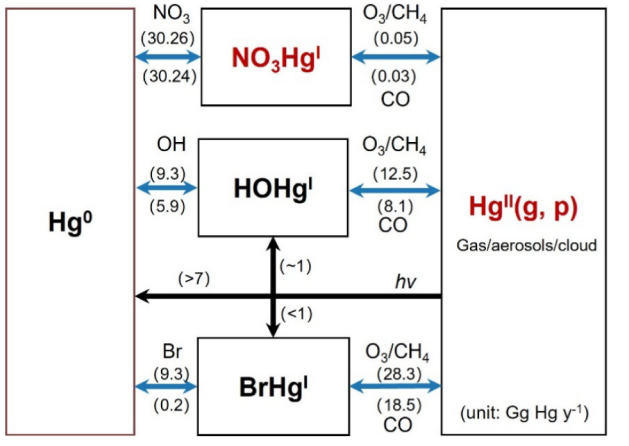

Figure 5. Main atmospheric Hg redox pathways including NO_3-initiated oxidation of GEM and subsequent redox reactions. Rates are in Gg Hg y^{-1}; values above and below the arrows are gross oxidation and reduction rates, respectively. Because Hg(II) can be rapidly reduced to Hg(I) and then oxidized to Hg(II), the rate of Hg(I) oxidation to Hg(II) exceeds the rate of oxidation of Hg(0) to Hg(I).

https://doi.org/10.1021/acsearthspacechem.5c00382
ACS Earth Space Chem. 2026, 10, 868−879

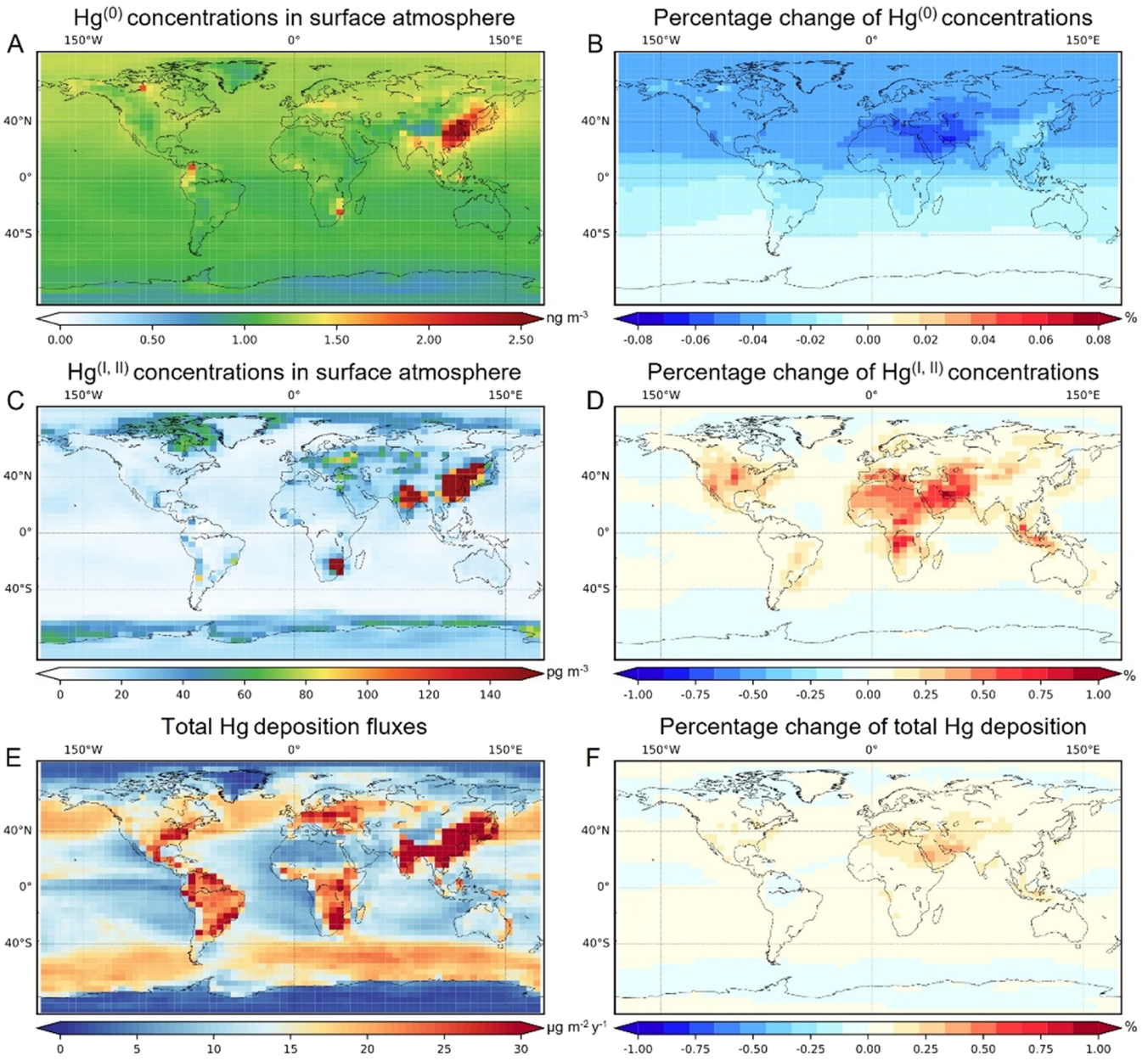

Figure 6. Spatial patterns of modeled results and changes in atmospheric Hg speciation and deposition when including the NO_3 chemistry pathway. Left panels (A, C, and E) depict modeled [Hg(0)], [Hg(I, II)], and total Hg deposition flux when adding NO_3-initiated oxidation of GEM chemistry reactions. Right-hand panels (B, D, and F) depict the corresponding percentage changes of Hg speciation and deposition caused by adding the NO_3 pathway to Shah-chemistry.

y^{-1}) occurs at a higher rate than by either Br or OH (both ~9 Gg y^{-1}), nearly all of the $NO_3Hg(I)\bullet$ intermediate product rapidly decomposes, effectively offsetting the NO_3-initiated oxidation of Hg(0). As a result, only a negligible fraction of $NO_3Hg(I)\bullet$ is converted to Hg(II), namely $NO_3Hg(II)O\bullet$ (~0.05 Gg y^{-1}), compared to oxidation rates of 12.5 Gg y^{-1} and 28.3 Gg y^{-1} for the OH- and Br-initiated pathways, respectively. Inclusion of the NO_3 pathway slightly decreases the global atmospheric Hg(0) reservoir from 4.58 Gg to 4.57 Gg and marginally increases the Hg(II) reservoir from 0.38 Gg to 0.39 Gg. These results indicate that NO_3 chemistry exerts a negligible influence on the global atmospheric mercury budget, reaffirming that Br and OH remain the dominant oxidants of atmospheric Hg(0), consistent with Shah et al.[3]

Our modeled atmospheric Hg budget differs from that of Shah et al. (2021). For example, the atmospheric Hg pool in our model contains 4.96 Gg, compared to 4.8 Gg in Shah et al. (2021). This discrepancy arises because our study simulates 2017, whereas Shah et al. (2021) simulated 2013−2015.

We further evaluated changes to the spatial distribution of atmospheric Hg when incorporating the NO_3 pathway. As shown in Figure 6, the model retains the same atmospheric Hg spatial patterns, concentrations, and deposition fluxes comparable to those simulated with the Shah et al. chemical mechanism (Figure 6A,C,E). Relative to the Shah chemistry, the inclusion of the NO_3 pathway does not alter the global mean surface Hg(0) concentration (1.14 ± 0.17 ng m^{-3}), the combined Hg(I, II) concentration (18.2 ± 41.9 pg m^{-3}), or the Hg(0) deposition flux (3.32 Gg y^{-1}), and only slightly

https://doi.org/10.1021/acsearthspacechem.5c00382
ACS Earth Space Chem. 2026, 10, 868−879

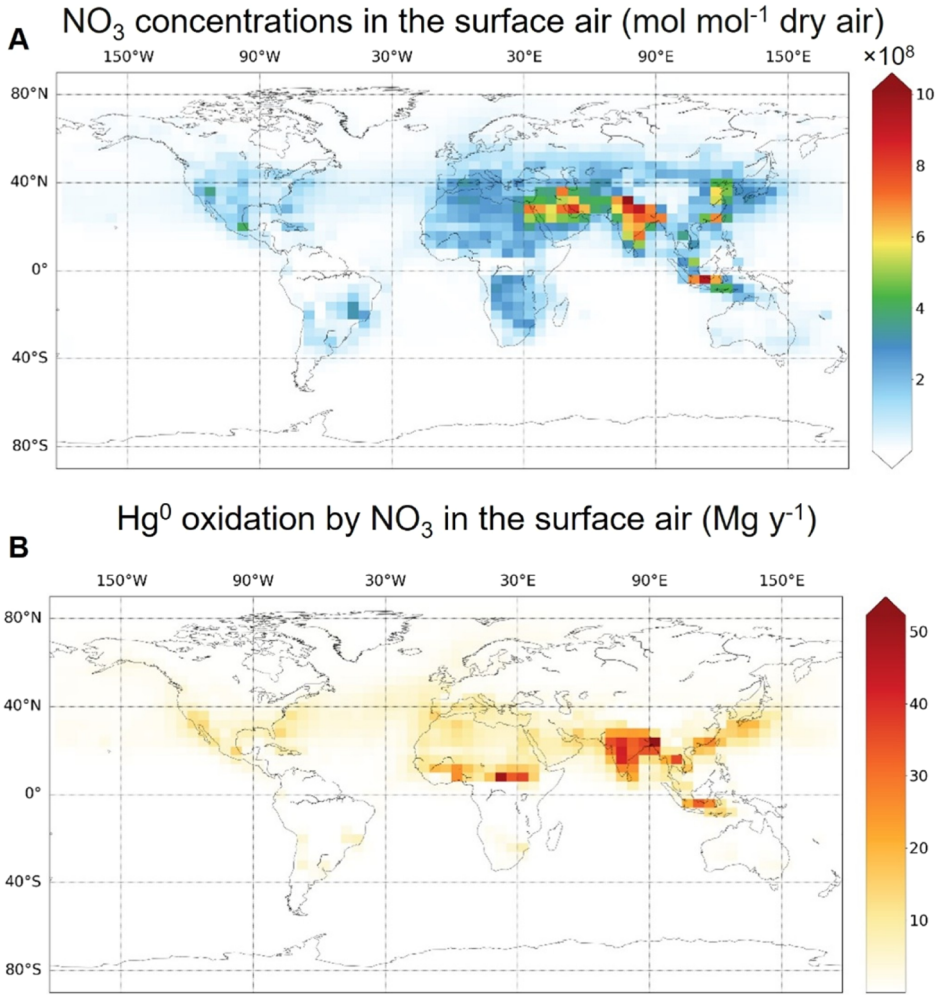

Figure 7. NO_3 concentrations and related oxidation rates in the model. (A) Annual mean NO_3 concentrations (mole fraction) in surface air. (B) Rates of Hg(0) oxidation by NO_3 to Hg(I)NO_3 in surface air. Surface air refers to the lowest atmospheric layer in the model, with an altitude of approximately 58 m above sea level.

increases total (wet + dry) Hg(II) deposition from 4.16 Gg y^{-1} to 4.18 Gg y^{-1}. Globally, the NO_3 pathway induces an average change of −0.02 ± 0.02% in surface Hg(0) concentrations, primarily in the Northern Hemisphere (Figure 6B), and a 0.05 ± 0.11% increase in Hg(I, II) concentrations, mainly over Africa, North America, and central−western Asia (Figure 6D). These regions coincide with elevated NO_3 levels, leading to slightly higher Hg(0) oxidation rates (Figure 7). Consequently, total atmospheric Hg (Hg(0) and Hg(II) deposition to the surface increases marginally by 0.03 ± 0.05% (Figure 6F), as Hg(II) species are more readily removed via wet and dry deposition than Hg(0). Overall, these findings demonstrate that the NO_3 pathway exerts minimal influence on the global atmospheric mercury cycle, consistent with our analysis of the field study by Peleg et al.

CONCLUSIONS

We have established that dissociation of the gas-phase $NO_3Hg(I)$• intermediate outcompetes bimolecular reactions that could transform it to Hg(II). This result undermines the rate constant determination by Sommar et al., and would need to be taken into account in any future study of the kinetics of NO_3 + Hg(0) → $NO_3Hg(I)$•. Fast dissociation of $NO_3Hg(I)$• means that reaction of nitrate radical with GEM cannot contribute significantly to oxidation of GEM to GOM in the troposphere, despite the much greater abundance of NO_3 than Br or OH, radicals which bind GEM more strongly than does NO_3 and dominate GEM oxidation to GOM. This finding would leave us without an explanation for the observations of Peleg et al., except for a very recent paper by Y. Wang et al.[23] Wang et al. observed strong correlations between nighttime production rates of NO_3 and enhancements in the fraction of GOM in total gaseous mercury at night (Δ%GOM). Along with temperature, their analysis identified [particulate nitrate] and PM_{10} as the next-most important variables correlating with Δ%GOM.[23] Wang et al. noted that reactions of NO_3 with halide ions at aerosol surfaces can produce Br and Cl,[105−107] both of which efficiently initiate oxidation of GEM to GOM. They incorporated this source of halogen atoms into a simplified kinetic model of GEM oxidation, and found remarkably good correlation between predicted and observed Δ%GOM. Their work suggests a potential explanation for the results of Peleg et al., since the present work shows that NO_3 cannot directly and efficiently initiate the direct oxidation of GEM in the gas phase.

https://doi.org/10.1021/acsearthspacechem.5c00382
ACS Earth Space Chem. 2026, 10, 868−879

■ ASSOCIATED CONTENT

Supporting Information

The Supporting Information is available free of charge at https://pubs.acs.org/doi/10.1021/acsearthspacechem.5c00382.

Absolute energies, ZPEs, cartesian coordinates, and vibrational frequencies for all species; reaction enthalpies; thermo input file and notes on vibrational frequencies used to calculate K_c; graphs of [$NO_3Hg(I)$•] and GOM production rates vs k_2 in simulations of fieldwork; the basis sets used in the SFX2C-1e-EOM-CC calculations for the NO_3Hg bond energy (PDF)

■ AUTHOR INFORMATION

Corresponding Authors

Zhengcheng Song − *State Key Laboratory of Environmental Geochemistry, Institute of Geochemistry, Chinese Academy of Sciences, Guiyang 550081, China*; Email: songzhengcheng@mail.gyig.ac.cn

Theodore S. Dibble − *Department of Chemistry, State University of New York, College of Environmental Science and Forestry, Syracuse, New York 13210, United States*; orcid.org/0000-0002-0023-8233; Email: tsdibble@esf.edu

Authors

Darshi T. Hewa Edirappulige − *Department of Chemistry, State University of New York, College of Environmental Science and Forestry, Syracuse, New York 13210, United States*; orcid.org/0009-0008-8538-1290

Lan Cheng − *Department of Chemistry, The Johns Hopkins University, Baltimore, Maryland 21218, United States*; orcid.org/0000-0003-1165-9559

Hang Du − *Nanjing-Helsinki Institute in Atmospheric and Earth System Sciences, Nanjing University, Nanjing 210023, China*

Pedro J. Castro − *Department of Chemistry, State University of New York, College of Environmental Science and Forestry, Syracuse, New York 13210, United States*; orcid.org/0000-0003-1650-4708

Yanxu Zhang − *Department of Earth and Environmental Sciences, Tulane University, New Orleans, Louisiana 70118, United States*

Complete contact information is available at: https://pubs.acs.org/10.1021/acsearthspacechem.5c00382

Notes

The authors declare no competing financial interest.

■ ACKNOWLEDGMENTS

Work at SUNY-ESF (D.H.T.E., P.J.C., & T.S.D.) was supported by the National Science Foundation under Grant 2004100. Work at Johns Hopkins University (L.C.) was supported by the Department of Energy, Office of Science, Office of Basic Energy Sciences under Award Number DE-SC0020317. Work at Nanjing University was supported by the National Natural Science Foundation of China (NSFC) 42394094. We thank an anonymous reviewer for their many suggestions, which helped improve the clarity of this paper.

■ REFERENCES

(1) Schroeder, W. H.; Munthe, J. Atmospheric mercury—An overview. *Atmos. Environ* **1998**, *32* (5), 809−822.

(2) Zhou, J.; Obrist, D. Global Mercury Assimilation by Vegetation. *Environ. Sci. Technol* **2021**, *55* (20), 14245−14257.

(3) Shah, V.; Jacob, D. J.; Thackray, C. P.; Wang, X.; Sunderland, E. M.; Dibble, T. S.; Saiz-Lopez, A.; Cernusák, I.; Kellö, V.; Castro, P. J.; Wu, R.; Wang, C. Improved Mechanistic Model of the Atmospheric Redox Chemistry of Mercury. *Environ. Sci. Technol* **2021**, *55* (21), 14445−14456.

(4) Saiz-Lopez, A.; Sitkiewicz, S. P.; Roca-Sanjuán, D.; Oliva-Enrich, J. M.; Dávalos, J. Z.; Notario, R.; Jiskra, M.; Xu, Y.; Wang, F.; Thackray, C. P.; Sunderland, E. M.; Jacob, D. J.; Travnikov, O.; Cuevas, C. A.; Acuña, A. U.; Rivero, D.; Plane, J. M. C.; Kinnison, D. E.; Sonke, J. E. Photoreduction of Gaseous Oxidized Mercury Changes Global Atmospheric Mercury Speciation, Transport and Deposition. *Nat. Commun* **2018**, *9* (1), 4796.

(5) Wu, R.; Castro, P. J.; Gaito, C.; Beiter, K.; Dibble, T. S.; Wang, C. Combined Experimental and Computational Kinetics Studies for the Atmospherically Important BrHg Radical Reacting with NO and O2. *J. Phys. Chem. A* **2022**, *126* (24), 3914−3925.

(6) Goodsite, M. E.; Plane, J. M. C.; Skov, H. A Theoretical Study of the Oxidation of Hg0 to HgBr2 in the Troposphere. *Environ. Sci. Technol* **2004**, *38* (6), 1772−1776.

(7) Jiao, Y.; Dibble, T. S. First Kinetic Study of the Atmospherically Important Reactions BrHg + NO2 and BrHg + HOO. *Phys. Chem. Chem. Phys* **2017**, *19* (3), 1826−1838.

(8) Dibble, T. S.; Zelie, M. J.; Mao, H. Thermodynamics of Reactions of ClHg and BrHg Radicals with Atmospherically Abundant Free Radicals. *Atmos. Chem. Phys* **2012**, *12* (21), 10271−10279.

(9) Dibble, T. S.; Zelie, M. J.; Mao, H. Erratum: Thermodynamics of Reactions of ClHg and BrHg Radicals with Atmospherically Abundant Free Radicals (Atmospheric Chemistry and Physics (2012) 12 (10271−10279)). *Atmos. Chem. Phys* **2013**, *13* (18), 9211.

(10) Wu, R.; Wang, C.; Dibble, T. S. First Experimental Kinetic Study of the Atmospherically Important Reaction of BrHg + NO2. *Chem. Phys. Lett* **2020**, *759*, 137928.

(11) Castro, P. J.; Kellö, V.; Cernušák, I.; Dibble, T. S. Together, Not Separately, OH and O3 Oxidize Hg(0) to Hg(II) in the Atmosphere. *J. Phys. Chem. A* **2022**, *126* (44), 8266−8279.

(12) Wu, L.; Mao, H.; Ye, Z.; Dibble, T. S.; Saiz-Lopez, A.; Zhang, Y. Improving Simulation of Gas-Particle Partitioning of Atmospheric Mercury Using CMAQ-newHg-Br V2. *J. Adv. Model. Earth Syst* **2024**, *16* (3), No. e2023MS003823.

(13) Dibble, T. S.; Tetu, H. L.; Jiao, Y.; Thackray, C. P.; Jacob, D. J. Modeling the OH-Initiated Oxidation of Mercury in the Global Atmosphere without Violating Physical Laws. *J. Phys. Chem. A* **2020**, *124* (2), 444−453.

(14) Horowitz, H. M.; Jacob, D. J.; Zhang, Y.; Dibble, T. S.; Slemr, F.; Amos, H. M.; Schmidt, J. A.; Corbitt, E. S.; Marais, E. A.; Sunderland, E. M. A New Mechanism for Atmospheric Mercury Redox Chemistry: Implications for the Global Mercury Budget. *Atmos. Chem. Phys* **2017**, *17*, 6353−6371.

(15) Wang, F.; Saiz-Lopez, A.; Mahajan, A. S.; Gómez Martín, J. C.; Armstrong, D.; Lemes, M.; Hay, T.; Prados-Roman, C. Enhanced Production of Oxidised Mercury over the Tropical Pacific Ocean: A Key Missing Oxidation Pathway. *Atmos. Chem. Phys* **2014**, *14* (3), 1323−1335.

(16) Francés-Monerris, A.; Carmona-García, J.; Acuña, A. U.; Dávalos, J. Z.; Cuevas, C. A.; Kinnison, D. E.; Francisco, J. S.; Saiz-Lopez, A.; Roca-Sanjuán, D. Photodissociation Mechanisms of Major Mercury(II) Species in the Atmospheric Chemical Cycle of Mercury. *Angew. Chem., Int. Ed* **2020**, *59*, 7605−7610.

(17) Saiz-Lopez, A.; Travnikov, O.; Sonke, J. E.; Thackray, C. P.; Jacob, D. J.; Carmona-García, J.; Francés-Monerris, A.; Roca-Sanjuán, D.; Acuña, A. U.; Dávalos, J. Z.; et al. Photochemistry of Oxidized Hg(I) and Hg(II) Species Suggests Missing Mercury Oxidation in the Troposphere. *Proc. Natl. Acad. Sci* **2020**, *117*, 30949−30956.

(18) Travnikov, O.; Angot, H.; Artaxo, P.; Bencardino, M.; Bieser, J.; D'Amore, F.; Dastoor, A.; De Simone, F.; Diéguez, M. D. C.; Dommergue, A. Multi-Model Study of Mercury Dispersion in the Atmosphere: Atmospheric Processes and Model Evaluation. *Atmos. Chem. Phys* **2017**, *17* (8), 5271−5295.
(19) Brown, S. S.; Stutz, J. Nighttime Radical Observations and Chemistry. *Chem. Soc. Rev* **2012**, *41* (19), 6405.
(20) Mao, H.; Talbot, R. W.; Sigler, J. M.; Sive, B. C.; Hegarty, J. D. Seasonal and Diurnal Variations of Hg° over New England. *Atmos. Chem. Phys* **2008**, *8* (5), 1403−1421.
(21) Weiss-Penzias, P.; Jaffe, D. A.; McClintick, A.; Prestbo, E. M.; Landis, M. S. Gaseous Elemental Mercury in the Marine Boundary Layer: Evidence for Rapid Removal in Anthropogenic Pollution. *Environ. Sci. Technol* **2003**, *37* (17), 3755−3763.
(22) Peleg, M.; Tas, E.; Obrist, D.; Matveev, V.; Moore, C.; Gabay, M.; Luria, M. Observational Evidence for Involvement of Nitrate Radicals in Nighttime Oxidation of Mercury. *Environ. Sci. Technol* **2015**, *49* (24), 14008−14018.
(23) Wang, Y.; Duan, Z.; Tang, Y.; Wang, S.; Li, Z.; Wang, Q.; Fu, J.; Wu, Q. Emerging Evidence of Nighttime Mercury Oxidation Driven by Nitrate Radical-Activated Heterogeneous Halogen Chemistry. *J. Hazard. Mater* **2026**, *501*, 140743.
(24) Sommar, J.; Hallquist, M.; Ljungström, E.; Lindqvist, O. On the Gas Phase Reactions Between Volatile Biogenic Mercury Species and the Nitrate Radical. *J. Atmos. Chem* **1997**, *27* (3), 233−247.
(25) Sumner, A. L.; Spicer, C. W.; Satola, J.; Mangaraj, R.; Cowen, K. A.; Landis, M. S.; Stevens, R. K.; Atkeson, T. D. Environmental Chamber Studies of Mercury Reactions in the Atmosphere. In *Dynamics of Mercury Pollution on Regional and Global Scales*; Springer-Verlag: New York, 2005, pp. 193−212. .
(26) Filatov, M.; Cremer, D. Revision of the Dissociation Energies of Mercury Chalcogenides−Unusual Types of Mercury Bonding. *ChemPhysChem* **2004**, *5* (10), 1547−1557.
(27) Cremer, D.; Kraka, E.; Filatov, M. Bonding in Mercury Molecules Described by the Normalized Elimination of the Small Component and Coupled Cluster Theory. *ChemPhysChem* **2008**, *9* (17), 2510−2521.
(28) Shepler, B. C.; Peterson, K. A. Mercury Monoxide: A Systematic Investigation of Its Ground Electronic State. *J. Phys. Chem. A* **2003**, *107* (11), 1783−1787.
(29) Peterson, K. A.; Shepler, B. C.; Singleton, J. M. The Group 12 Metal Chalcogenides: An Accurate Multireference Configuration Interaction and Coupled Cluster Study. *Mol. Phys* **2007**, *105* (9), 1139−1155.
(30) Hynes, A. J.; Donohoue, D. L.; Goodsite, M. E.; Hedgecock, I. M. Our Current Understanding of Major Chemical and Physical Processes Affecting Mercury Dynamics in the Atmosphere and at the Air-Water/Terrestrial Interfaces. In *Mercury Fate and Transport in the Global Atmosphere: Emissions, Measurements and Models*; Springer US, 2009, pp. 427−457.
(31) Viel, A.; Eisfeld, W. NO3 Full-Dimensional Potential Energy Surfaces and Ground State Vibrational Levels Revisited. *Chem. Phys* **2018**, *509*, 81−90.
(32) Eisfeld, W.; Morokuma, K. A Detailed Study on the Symmetry Breaking and Its Effect on the Potential Surface of NO3. *J. Chem. Phys* **2000**, *113* (14), 5587−5597.
(33) Mayer, M.; Cederbaum, L. S.; Köppel, H. Ground State Dynamics of NO3: Multimode Vibronic Borrowing Including Thermal Effects. *J. Chem. Phys* **1994**, *100* (2), 899−911.
(34) Stanton, J. F.; Gauss, J.; Bartlett, R. J. On the Choice of Orbitals for Symmetry Breaking Problems with Application to NO3. *J. Chem. Phys* **1992**, *97* (8), 5554−5559.
(35) Stanton, J. F.; Gauss, J.; Bartlett, R. J. Potential Nonrigidity of the NO3 Radical. *J. Chem. Phys* **1991**, *94* (5), 4084−4087.
(36) Kim, B.; Johnston, H. S.; Clabo, D. A.; Schaefer, H. F. Vertical Electronic Spectrum of NO3: 2 A'2, 2 E''(2 A 2,2 B 1), and 2 E' States. *J. Chem. Phys* **1988**, *88* (5), 3204−3210.
(37) Gómez Martín, J. C.; Lewis, T. R.; Douglas, K. M.; Blitz, M. A.; Saiz-Lopez, A.; Plane, J. M. C. The Reaction between HgBr and O3: Kinetic Study and Atmospheric Implications. *Phys. Chem. Chem. Phys* **2022**, *24* (20), 12419−12432.
(38) Cohen, R. W.; Ovitigala, A.; Wang, C.; Dibble, T. S. Temperature and Pressure Dependence of the Reaction between BrHg and O3. *Chem. Phys. Lett* **2025**, *878*, 142373.
(39) Bauer, D.; Donohoue, D.; Hynes, A. A Pulsed Laser Photolysis − Pulsed Laser Induced Fluorescence Study of the Kinetics and Mechanism of the Reaction of HgBr with NO2 and O2. *Environ. Sci.: Atmos* **2025**, *5* (5), 636−647.
(40) Khan, M. A. H.; Cooke, M. C.; Utembe, S. R.; Archibald, A. T.; Derwent, R. G.; Xiao, P.; Percival, C. J.; Jenkin, M. E.; Morris, W. C.; Shallcross, D. E. Global Modeling of the Nitrate Radical (NO3) for Present and Pre-Industrial Scenarios. *Atmos. Res* **2015**, *164*−*165*, 347−357.
(41) Rosanka, S.; Vu, G. H. T.; Nguyen, H. M. T.; Pham, T. V.; Javed, U.; Taraborrelli, D.; Vereecken, L. Atmospheric Chemical Loss Processes of Isocyanic Acid (HNCO): A Combined Theoretical Kinetic and Global Modelling Study. *Atmos. Chem. Phys* **2020**, *20* (11), 6671−6686.
(42) Chua, G.; Naik, V.; Horowitz, L. W. Exploring the Drivers of Tropospheric Hydroxyl Radical Trends in the Geophysical Fluid Dynamics Laboratory AM4.1 Atmospheric Chemistry−Climate Model. *Atmos. Chem. Phys* **2023**, *23* (8), 4955−4975.
(43) Penkett, S. A.; Burgess, R. A.; Coe, H.; Coll, I.; Hov, Ø.; Lindskog, A.; Schmidbauer, N.; Solberg, S.; Roemer, M.; Thijsse, T.; Beck, J.; Reeves, C. E. Evidence for Large Average Concentrations of the Nitrate Radical (NO3) in Western Europe from the HANSA Hydrocarbon Database. *Atmos. Environ* **2007**, *41* (16), 3465−3478.
(44) Stanton, J. F.; Bartlett, R. J. The Equation of Motion Coupled-Cluster Method. A Systematic Biorthogonal Approach to Molecular Excitation Energies, Transition Probabilities, and Excited State Properties. *J. Chem. Phys* **1993**, *98* (9), 7029−7039.
(45) Stanton, J. F.; Gauss, J. Analytic Energy Derivatives for Ionized States Described by the Equation-of-Motion Coupled Cluster Method. *J. Chem. Phys* **1994**, *101* (10), 8938−8944.
(46) Stanton, J. F. On the Vibronic Level Structure in the NO3 Radical. I. The Ground Electronic State. *J. Chem. Phys* **2007**, *126* (13), 134309.
(47) Stanton, J. F. On the Vibronic Level Structure in the NO3 Radical: II. Adiabatic Calculation of the Infrared Spectrum. *Mol. Phys* **2009**, *107* (8−12), 1059−1075.
(48) Stanton, J. F.; Gauss, J. A Simple Scheme for the Direct Calculation of Ionization Potentials with Coupled-Cluster Theory That Exploits Established Excitation Energy Methods. *J. Chem. Phys* **1999**, *111* (19), 8785−8788.
(49) Matthews, D. A.; Stanton, J. F. Non-Orthogonal Spin-Adaptation of Coupled Cluster Methods: A New Implementation of Methods Including Quadruple Excitations. *J. Chem. Phys* **2015**, *142* (6), 064108.
(50) Dyall, K. G. Interfacing Relativistic and Nonrelativistic Methods. IV. One- and Two-Electron Scalar Approximations. *J. Chem. Phys* **2001**, *115* (20), 9136−9143.
(51) Liu, W.; Peng, D. Exact Two-Component Hamiltonians Revisited. *J. Chem. Phys* **2009**, *131* (3), 031104.
(52) Cheng, L.; Gauss, J. Analytic Energy Gradients for the Spin-Free Exact Two-Component Theory Using an Exact Block Diagonalization for the One-Electron Dirac Hamiltonian. *J. Chem. Phys* **2011**, *135* (8), 084114.
(53) Roos, B. O.; Malmqvist, P.-Å.; Veryazov, V.; Widmark, P.-O. Main Group Atoms and Dimers Studied with a New Relativistic ANO Basis Set. *J. Phys. Chem. A* **2004**, *108* (15), 2851−2858.
(54) Faegri, K., Jr. Relativistic Gaussian Basis Sets for the Elements K - Uuo. *Theor. Chem. Acc.* **2001**, *105* (3), 252−258.
(55) Roos, B. O.; Lindh, R.; Malmqvist, P.-Å.; Veryazov, V.; Widmark, P.-O. New Relativistic ANO Basis Sets for Transition Metal Atoms. *J. Phys. Chem. A* **2005**, *109* (29), 6575−6579.
(56) Peterson, K. A.; Puzzarini, C. Systematically Convergent Basis Sets for Transition Metals. II. Pseudopotential-Based Correlation

Consistent Basis Sets for the Group 11 (Cu, Ag, Au) and 12 (Zn, Cd, Hg) Elements. *Theor. Chem. Acc* **2005**, *114* (4−5), 283−296.
(57) Kendall, R. A.; Dunning, T. H.; Harrison, R. J. Electron Affinities of the First-row Atoms Revisited. Systematic Basis Sets and Wave Functions. *J. Chem. Phys* **1992**, *96* (9), 6796−6806.
(58) Helgaker, T.; Klopper, W.; Koch, H.; Noga, J. Basis-Set Convergence of Correlated Calculations on Water. *J. Chem. Phys* **1997**, *106* (23), 9639−9646.
(59) Kutzelnigg, W.; Liu, W. Quasirelativistic Theory Equivalent to Fully Relativistic Theory. *J. Chem. Phys* **2005**, *123* (24), 241102.
(60) Heß, B. A.; Marian, C. M.; Wahlgren, U.; Gropen, O. A Mean-Field Spin-Orbit Method Applicable to Correlated Wavefunctions. *Chem. Phys. Lett* **1996**, *251* (5−6), 365−371.
(61) Liu, J.; Cheng, L. An Atomic Mean-Field Spin-Orbit Approach within Exact Two-Component Theory for a Non-Perturbative Treatment of Spin-Orbit Coupling. *J. Chem. Phys* **2018**, *148* (14), 144108.
(62) Zhang, C.; Cheng, L. Atomic Mean-Field Approach within Exact Two-Component Theory Based on the Dirac−Coulomb−Breit Hamiltonian. *J. Phys. Chem. A* **2022**, *126* (27), 4537−4553.
(63) Asthana, A.; Liu, J.; Cheng, L. Exact Two-Component Equation-of-Motion Coupled-Cluster Singles and Doubles Method Using Atomic Mean-Field Spin-Orbit Integrals. *J. Chem. Phys* **2019**, *150* (7), 074102.
(64) Matthews, D. A.; Cheng, L.; Harding, M. E.; Lipparini, F.; Stopkowicz, S.; Jagau, T.-C.; Szalay, P. G.; Gauss, J.; Stanton, J. F. Coupled-Cluster Techniques for Computational Chemistry: The CFOUR Program Package. *J. Chem. Phys.* **2020**, *152*, 214108.
(65) Barker, J. R. Multiple-Well, Multiple-Path Unimolecular Reaction Systems. I. MultiWell Computer Program Suite. *Int. J. Chem. Kinet* **2001**, *33* (4), 232−245.
(66) Barker, J. R.; Nguyen, T. L.; Stanton, J. F.; Aieta, C.; Ceotto, M.; Gabas, F.; Kumar, T. J. D.; Li, C. G. L.; Lohr, L. L.; Maranzana, A., et al. *MultiWell-2023 Software Suite*. University of Michigan, Ann Arbor 2023.
(67) Barker, J. R. Energy Transfer in Master Equation Simulations: A New Approach. *Int. J. Chem. Kinet* **2009**, *41* (12), 748−763.
(68) Frisch, M. J.; Trucks, G. W.; Schlegel, H. B.; Scuseria, G. E.; Robb, M. A.; Cheeseman, J. R.; Scalmani, G.; Barone, V.; Petersson, G. A.; Nakatsuji, H.; et al. *Gaussian 16, Rev. A.* Gaussian, Inc.: 2016.
(69) Neese, F. The ORCA Program System. *WIREs Comput. Mol. Sci* **2012**, *2* (1), 73−78.
(70) Neese, F. Software Update: The ORCA Program System—Version 5.0. *WIREs Comput. Mol. Sci* **2022**, *12* (5), No. e1606.
(71) Yanai, T.; Tew, D. P.; Handy, N. C. A New Hybrid Exchange−Correlation Functional Using the Coulomb-Attenuating Method (CAM-B3LYP). *Chem. Phys. Lett* **2004**, *393* (1−3), 51−57.
(72) Grimme, S.; Ehrlich, S.; Goerigk, L. Effect of the Damping Function in Dispersion Corrected Density Functional Theory. *J. Comput. Chem* **2011**, *32* (7), 1456−1465.
(73) Adamo, C.; Barone, V. Toward Reliable Density Functional Methods without Adjustable Parameters: The PBE0Model. *J. Chem. Phys* **1999**, *110* (13), 6158−6170.
(74) Zhao, Y.; Truhlar, D. G. The M06 Suite of Density Functionals for Main Group Thermochemistry, Thermochemical Kinetics, Noncovalent Interactions, Excited States, and Transition Elements: Two New Functionals and Systematic Testing of Four M06-Class Functionals and 12 Other Functionals. *Theor. Chem. Acc* **2008**, *120* (1−3), 215−241.
(75) Dunning, T. H. Gaussian Basis Sets for Use in Correlated Molecular Calculations. I. The Atoms Boron through Neon and Hydrogen. *J. Chem. Phys* **1989**, *90* (2), 1007−1023.
(76) Peterson, K. A.; Dunning, T. H. Accurate Correlation Consistent Basis Sets for Molecular Core-Valence Correlation Effects: The Second Row Atoms Al-Ar, and the First Row Atoms B-Ne Revisited. *J. Chem. Phys* **2002**, *117* (23), 10548−10560.
(77) Peterson, K. A.; Figgen, D.; Goll, E.; Stoll, H.; Dolg, M. Systematically Convergent Basis Sets with Relativistic Pseudopotentials. II. Small-Core Pseudopotentials and Correlation Consistent Basis Sets for the Post-d Group 16−18 Elements. *J. Chem. Phys* **2003**, *119* (21), 11113.
(78) Figgen, D.; Rauhut, G.; Dolg, M.; Stoll, H. Energy-Consistent Pseudopotentials for Group 11 and 12 Atoms: Adjustment to Multi-Configuration Dirac−Hartree−Fock Data. *Chem. Phys* **2005**, *311* (1−2), 227−244.
(79) Jiao, Y.; Dibble, T. S. Quality Structures, Vibrational Frequencies, and Thermochemistry of the Products of Reaction of BrHg with NO2, HO2, ClO, BrO, and IO. *J. Phys. Chem. A* **2015**, *119* (42), 10502−10510.
(80) Dixon, D. A.; Peterson, K. A.; Francisco, J. S. The Molecular Structures and Energetics of Cl2 CO, ClCO, Br2 CO, and BrCO. *J. Phys. Chem. A* **2000**, *104* (26), 6227−6232.
(81) The International GEOS-Chem User Community. *geoschem/geos-chem: GEOS-Chem 12.9.0* Zenodo 2020. https://zenodo.org/records/3950327 Accessed 26 October 2025.
(82) Streets, D. G.; Horowitz, H. M.; Lu, Z.; Levin, L.; Thackray, C. P.; Sunderland, E. M. Global and Regional Trends in Mercury Emissions and Concentrations, 2010−2015. *Atmos. Environ* **2019**, *201*, 417−427.
(83) Zhang, Y.; Zhang, P.; Song, Z.; Huang, S.; Yuan, T.; Wu, P.; Shah, V.; Liu, M.; Chen, L.; Wang, X.; Zhou, J.; Agnan, Y. An Updated Global Mercury Budget from a Coupled Atmosphere-Land-Ocean Model: 40% More Re-Emissions Buffer the Effect of Primary Emission Reductions. *One Earth* **2023**, *6*, 316−325.
(84) Wesely, M. Parameterization of Surface Resistances to Gaseous Dry Deposition in Regional-Scale Numerical Models☆. *Atmos. Environ* **2007**, *41*, 52−63.
(85) Strode, S. A.; Jaeglé, L.; Selin, N. E.; Jacob, D. J.; Park, R. J.; Yantosca, R. M.; Mason, R. P.; Slemr, F. Air-sea Exchange in the Global Mercury Cycle. *Global Biogeochem. Cycles* **2007**, *21* (1), GB1017.
(86) Liu, H.; Jacob, D. J.; Bey, I.; Yantosca, R. M. Constraints from 210 Pb and 7 Be on Wet Deposition and Transport in a Global Three-dimensional Chemical Tracer Model Driven by Assimilated Meteorological Fields. *J. Geophys. Res.: Atmos* **2001**, *106* (D11), 12109−12128.
(87) Zhang, L.; Gong, S.; Padro, J.; Barrie, L. A Size-Segregated Particle Dry Deposition Scheme for an Atmospheric Aerosol Module. *Atmos. Environ* **2001**, *35* (3), 549−560.
(88) Amos, H. M.; Jacob, D. J.; Holmes, C. D.; Fisher, J. A.; Wang, Q.; Yantosca, R. M.; Corbitt, E. S.; Galarneau, E.; Rutter, A. P.; Gustin, M. S.; Steffen, A.; Schauer, J. J.; Graydon, J. A.; Louis, V. L. S.; Talbot, R. W.; Edgerton, E. S.; Zhang, Y.; Sunderland, E. M. Gas-Particle Partitioning of Atmospheric Hg(II) and Its Effect on Global Mercury Deposition. *Atmos. Chem. Phys* **2012**, *12* (1), 591−603.
(89) The International GEOS-Chem User Community. *GEOS-Chem. 14.5.1* Zenodo 2025. https://github.com/geoschem/GCClassic/releases/tag/14.5.1 Accessed 26 October 2025.
(90) Barker, J. R.; Nguyen, T. L.; Stanton, J. F.; Aieta, C.; Ceotto, M.; Gabas, F.; Kumar, T. J. D.; Li, C. G. L.; Lohr, L. L.; Maranzana, A., et al. *MultiWell-2019 Software Suite*; University of Michigan; Ann Arbor, Michigan, USA, 2019.
(91) Langer, S.; Ljungström, E.; Wängberg, I. Rates of Reaction between the Nitrate Radical and Some Aliphatic Esters. *J. Chem. Soc., Faraday Trans* **1993**, *89* (3), 425−431.
(92) Ianni, J. C. Kintecus, www.kintecus.com. 2019.
(93) Ianni, J. C. A Comparison of the Bader-Deuflhard and the Cash-Karp Runge-Kutta Integrators for the GRI-MECH 3.0 Model Based on the Chemical Kinetics Code Kintecus. In *Computational Fluid and Solid Mechanics 2003; Proceedings Second MIT Conference on Compurational Fluid and Solid Mechanics*; Elsevier, 2003, pp. 1368−1372. .
(94) Lam, K. T.; Wilhelmsen, C. J.; Dibble, T. S. BrHgO• + C2H4 and BrHgO• + HCHO in Atmospheric Oxidation of Mercury: Determining Rate Constants of Reactions with Pre-Reactive Complexes and a Bifurcation. *J. Phys. Chem. A* **2019**, *123*, 6045−6055.
(95) Lam, K. T.; Wilhelmsen, C. J.; Schwid, A. C.; Jiao, Y.; Dibble, T. S. Computational Study on the Photolysis of BrHgONO and the

Reactions of BrHgO• with CH4, C2H6, NO, and NO2: Implications for Formation of Hg(II) Compounds in the Atmosphere. *J. Phys. Chem. A* **2019**, *123* (8), 1637−1647.
(96) Hewa Edirappulige, D. T.; Kirby, I. J.; Beckett, C. K.; Dibble, T. S. Atmospheric Chemistry of HOHg(II)O• Mimics That of a Hydroxyl Radical. *J. Phys. Chem. A* **2023**, *127* (40), 8392−8403.
(97) Khiri, D.; Louis, F.; Cernusak, I.; Dibble, T. BrHgO• + CO: Analogue of OH + CO and Reduction Path for Hg(II) in the Atmosphere. *ACS Earth Space Chem* **2020**, *4* (10), 1777−1784.
(98) Donohoue, D. L.; Bauer, D.; Cossairt, B.; Hynes, A. J. Temperature and Pressure Dependent Rate Coefficients for the Reaction of Hg with Br and the Reaction of Br with Br: A Pulsed Laser Photolysis-Pulsed Laser Induced Fluorescence Study. *J. Phys. Chem. A* **2006**, *110*, 6623−6632.
(99) Sommar, J.; Gårdfeldt, K.; Strömberg, D.; Feng, X. A Kinetic Study of the Gas-Phase Reaction between the Hydroxyl Radical and Atomic Mercury. *Atmos. Environ* **2001**, *35* (17), 3049−3054.
(100) Pal, B.; Ariya, P. A. Gas-Phase HO-Initiated Reactions of Elemental Mercury: Kinetics, Product Studies, and Atmospheric Implications. *Environ. Sci. Technol* **2004**, *38* (21), 5555−5566.
(101) Gustin, M. S.; Dunham-Cheatham, S. M.; Lyman, S.; Horvat, M.; Gay, D. A.; Gačnik, J.; Gratz, L.; Kempkes, G.; Khalizov, A.; Lin, C.-J.; Lindberg, S. E.; Lown, L.; Martin, L.; Mason, R. P.; MacSween, K.; Vijayakumaran Nair, S.; Nguyen, L. S. P.; O'Neil, T.; Sommar, J.; Weiss-Penzias, P.; Zhang, L.; Živković, I. Measurement of Atmospheric Mercury: Current Limitations and Suggestions for Paths Forward. *Environ. Sci. Technol* **2024**, *58* (29), 12853−12864.
(102) Huang, J.; Miller, M. B.; Weiss-Penzias, P.; Gustin, M. S. Comparison of Gaseous Oxidized Hg Measured by KCl-Coated Denuders, and Nylon and Cation Exchange Membranes. *Environ. Sci. Technol* **2013**, *47* (13), 7307−7316.
(103) He, Y.; Mason, R. P. Comparison of Reactive Gaseous Mercury Measured by KCl-Coated Denuders and Cation Exchange Membranes during the Pacific GEOTRACES GP15 Expedition. *Atmos. Environ* **2021**, *244*, 117973.
(104) Marusczak, N.; Sonke, J. E.; Fu, X.; Jiskra, M. Tropospheric GOM at the Pic Du Midi Observatory—Correcting Bias in Denuder Based Observations. *Environ. Sci. Technol* **2017**, *51* (2), 863−869.
(105) Rudich, Y.; Talukdar, R. K.; Ravishankara, A. R.; Fox, R. W. Reactive Uptake of NO 3 on Pure Water and Ionic Solutions. *J. Geophys. Res.: Atmos* **1996**, *101* (D15), 21023−21031.
(106) Seisel, S.; Caloz, F.; Fenter, F. F.; van den Bergh, H.; Rossi, M. J. The Heterogeneous Reaction of NO 3 with NaCl and KBr: A Nonphotolytic Source of Halogen Atoms. *Geophys. Res. Lett* **1997**, *24* (22), 2757−2760.
(107) Gershenzon, M. Y.; Il'in, S.; Fedotov, N. G.; Gershenzon, Y. M.; Aparina, E. V.; Zelenov, V. V. The Mechanism of Reactive NO3 Uptake on Dry NaX (X = Cl, Br). *J. Atmos. Chem* **1999**, *34* (1), 119−135.

https://doi.org/10.1021/acsearthspacechem.5c00382
ACS Earth Space Chem. 2026, 10, 868−879